Vorticity on a Barred Beach

Tivon Jacobson

1 Introduction

Longshore current modeling has been dominated by a radiation-stress viewpoint applied to shallow-water models. While the shallow-water model is arguably appropriate for gently sloping beaches, radiation-stress convergences are difficult to apply directly in the momentum equations when longshore (y-coordinate) inhomogeneities are present. To date, longshore currents have been modelled with y-independent wave forcing. Should longshore inhomogeneities be fundamental to surf zone dynamics, the traditional models are insufficient. This has been pointed out in articles by D.H. Peregrine ([1], [2]), and was brought to our attention by F. Feddersen. [3]

Feddersen mentioned the problem of longshore currents on a barred beach. (Figure 1) There, waves breaking over bar and beach have their radiation stress convergences in these locations. The y-independent theory predicts the development of longshore currents over the bar and on the beach, a forecast at variance with observation. Experiments on a barred beach in North Carolina found the longshore current in the trough between bar and beach. [4] Laboratory experiments (and our numerical experiments of section 6) find that with wave forcing which does not depend on y, the longshore currents indeed do develop over bar and beach. Inhomogeneous forcing is a candidate to explain the observations.

Some theoretical difficulties with y-dependence may be overcome by considering vorticity forcing rather than radiation stress convergence. The vorticity sources are those due to wave breaking. With a sense of the location and strength of these vorticity sources, the problem becomes one of predicting the vortex dynamics which result. A first approximation for the location of the vorticity sources can be had using WKB theory and a parameterization of breaking. As well, Peregrine has derived a strength for such vortex sources using the circulation integral. [1] We found the Generalized Lagrangian Mean theory useful in

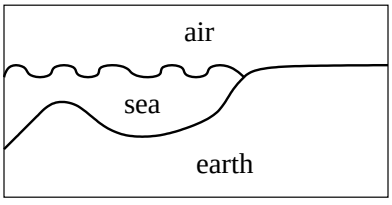

Figure 1: A Barred Beach.

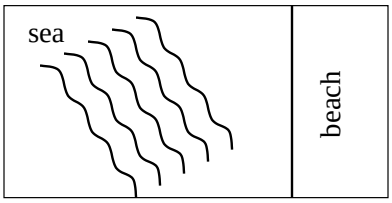

Figure 2: A wavetrain incident at an angle.

determination of these strengths, and discuss this in section 4. Some simple results which are helpful in predicting vortex dynamics are presented in section 5.

A numerical model of the surf zone was used to resolve wave and vorticity alike. The model was a 2D, finite-volume, shock-resolving shallow water model with varying bottom topography. The use of such a model to simulate vortex dynamics was expensive in computation time, since the gravity wave speeds provide a severe CFL restriction on the time-stepping. Nevertheless, this model reperesents a means by which the entire wave-forcing process may be represented without parameterization.

The wave-forcing was considered to be by a wavetrain with longshore envelope incident on the beach at an angle. (Figure 2) We found that simple vortex dynamics predict a longshore current in the trough. This prediction was confirmed with the numerical model.

2 Equations of Motion in Shallow Waters

We will use a shallow water model for the surfzone throughout this article. Here we present the shallow-water equations for reference. Figure 3 shows the meaning of the variables.

$$u_{,t} + uu_{,x} + vu_{,y} = -c_{00}^2(h_{,x} + h_{b,x}) \quad (1)$$

$$v_{,t} + uv_{,x} + vv_{,y} = -c_{00}^2(h_{,y} + h_{b,y}) \quad (2)$$

$$h_{,t} + (hu)_{,x} + (hv)_{,y} = 0. \quad (3)$$

The variable x represents cross-shore distances, the variable y alongshore distances. This is a nondimensionalized model with the gravity g and constant reference depth H factored into $c_{00} = \sqrt{gH}$. No apologies are made for the use of the shallow-water model, although we note several modeling limitations in section 6. While the use of shallow-water bores as a model of ocean-wave breaking lacks in its description of the breaking wave region itself, the location and rough magnitude of vorticity sources due to breaking are of more interest in this article. Moreover, precise models of wave-breaking may be desirable, but a 3D free-surface simulation of the surf zone is well beyond analytical or computational means. It is not beyond experimental means: wavetanks capable of such simulations exist. [5]

Our shallow-water model has no explicit viscous contribution. Viscous momentum mixing and bottom drag necessarily enter the longshore current picture in the forced-dissipative mean-state. We limit our concern to the initial transferral of wave-induced momentum change to the trough region. However the addition of bottom friction to the model is straightforward and we intend to carry this out in future work.

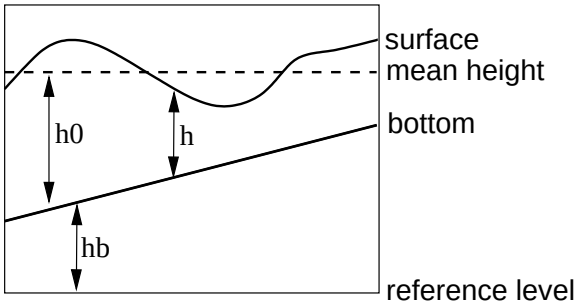

Figure 3: The Shallow Water Model.

3 Ray Tracing

Ray-tracing provides for approximate calculation of the wave amplitudes. These may be used in estimating vorticity source terms. We develop some ray-trace formulae and apply them as needed. A full development of these methods can be found in many places, such as [6]. An example of the use of this method to calculate vorticity sources may be found in [7]. Throughout, we assume that the mean flow has no effect on the waves. Generalizations of the method exist to deal with such a case, but the situation then becomes much more complex.

For frequency ω and wavenumber vector $\vec{k}$, we have:

$$\vec{k}_{,t} + \vec{c_g} \cdot \nabla_x \vec{k} = -\nabla_x \omega, \tag{4}$$

$$\omega_{,t} + \vec{c_g} \cdot \nabla_x \omega = -\omega_{,t}. \tag{5}$$

Here, $\omega = \omega(\vec{k}, \vec{x}, t)$ is the frequency. The dependence of ω on the wavenumber vector, the position and the time constitutes the dispersion relation. To find a law for the amplitude of the waves, one can take as starting point the conservation of wave-action ([8]) to arrive at:

$$\left(\frac{h_0 E}{\omega}\right)_{,t} + \nabla_x \cdot \left(\vec{c_g} \frac{h_0 E}{\omega}\right) = -D(h_0, E). \tag{6}$$

The quantity E is the wave energy density per unit mass. The function $D(h_0, E)$ is a dissipation which represents the effect of loss of wave energy due to breaking. For shallow water,

$$\omega(\vec{k}, \vec{x}, t) = c_{00}\sqrt{h_0(\vec{x})}|\vec{k}|, \tag{7}$$

$$E = \frac{1}{2}(|u|^2 + c_{00}^2 \frac{(\Delta h)^2}{h_0(\vec{x})}). \tag{8}$$

The quantity Δh is the surface perturbation $(h - h_0)$. (See Figure 3) For linear monochromatic waves, we could replace Δh by a harmonically varying wave height h'. The polarization realtions for the linear wave then give

$$E = \frac{c_{00}^2}{h_0}\overline{h'^2}. \tag{9}$$

In our case there will be no topographic dependence on y. The dispersion relation is time-independent. As a consequence, equations 4 reduce to:

$$\begin{aligned} k_{,t} + c_{gx}k_{,x} &= -\omega_{,x} && (10)\\ l &= l_0, \text{ constant along rays} && (11)\\ \omega &= \omega_0, \text{ constant along rays} && (12)\\ \omega_0 &= c_{00}\sqrt{h_0(x)}\sqrt{k^2 + l_0^2}. && (13) \end{aligned}$$

The last three are sufficient to find the trajectories of rays, since rays are the integral curves of the group velocity, a function of k, l, ω. The integration of the wave energy density by equation 6 can now be contemplated if the field of group velocities is known. From the field of wave energy density will come the vorticity source terms (Section 4).

Calculation of the wave energy density must take breaking into account. Consider the case in which the waves have reached a forced-dissipative equilibrium. We also assume independence of y for expository purposes, so that the average square linear wave amplitude $\overline{h'^2}$ in given (via equation 6 and 9) in terms of the bottom topography:

$$\left(\sqrt{h_0}\ \overline{h'^2}\right)_{,x} = -\frac{\omega_0}{c_{00}^3}D(E, h_0). \tag{14}$$

Assuming that the waves break only when the nonlinear amplitides are large enough, $(\sqrt{h_0}\ \overline{h'^2})_{,x} = 0$ in non-breaking regions. The assumption is ad-hoc, but captures that we wish to see sudden transitions to wave-breaking over topographic features. One could introduce an additional law for the scaling of wave amplitude in breaking regions and integrate equation 14 to get the energy density or mean-square amplitude field.

Figure 4 shows the cross-shore wave amplitudes (without breaking) in the case in which it is assumed that the waves have no alongshore envelope.

4 Vorticity Sources, GLM, and the Circulation Theorem

A presentation of Generalized Lagrangian Mean (GLM) theory may be found in the two papers by Andrews and McIntyre ([8], [9]). Some additional information about the theory, as well as examples of its application to the theory of breaking waves are in [10], [7]. Of essential interest to us is that GLM gives an approximate expession for the time rate of change of mean vorticity in terms of the evolution of the wave pseudomomentum. We have since found that the same results are available from the curl of the radiation-stress tensor expressed in terms of the infinitesimal waves. The exact finite amplitude equations are difficult to interpret in the present case, but rough estimates for sources in the breaking region in terms of infinitesimal wave quantities are available [7]:

$$(\nabla \times \overline{u})_{,t} = \nabla \times \vec{\mathcal{F}}, \tag{15}$$

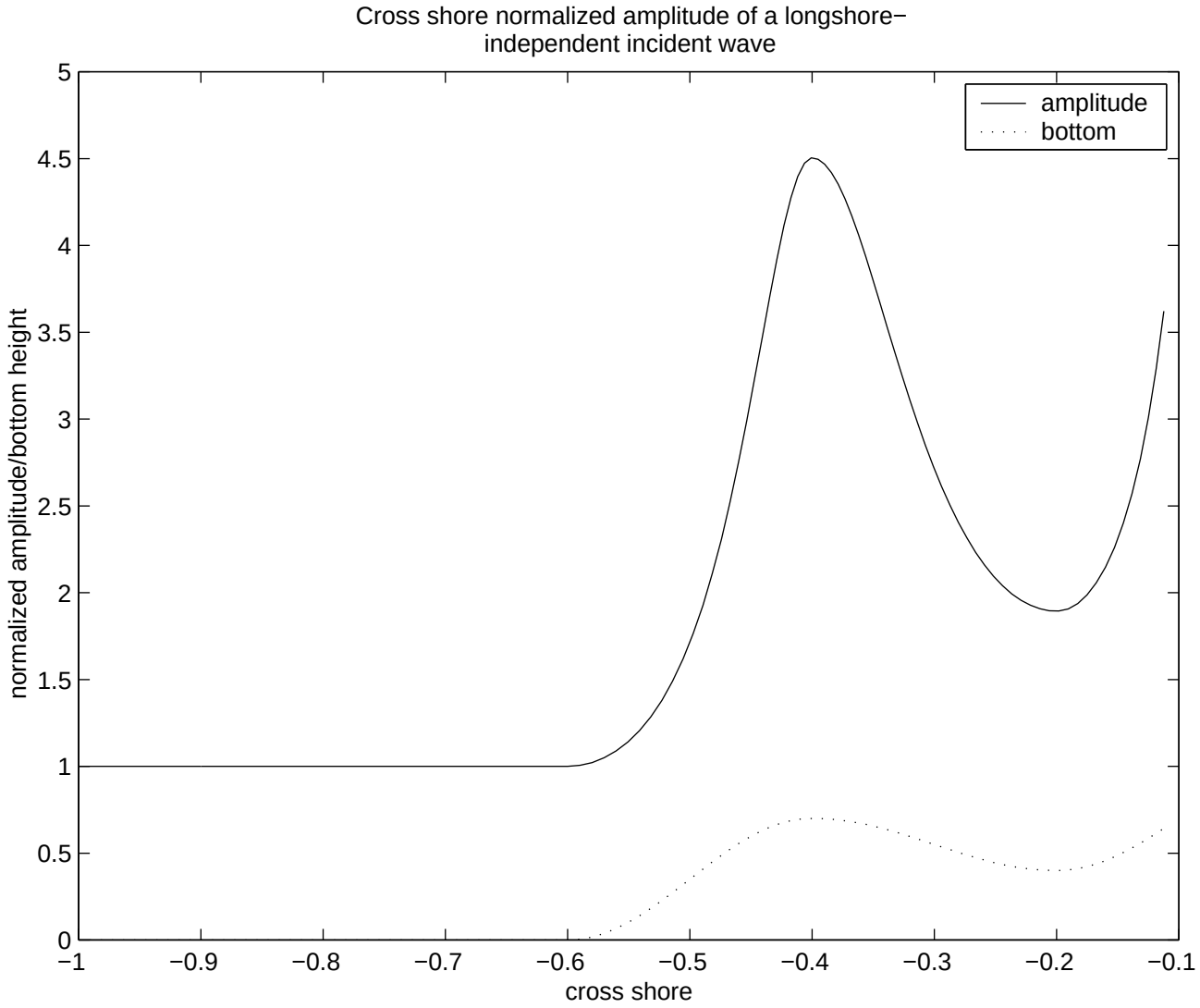

Figure 4: Example of Cross-Shore Amplitudes.

$$\mathcal{F}_x = \frac{k}{h_0}\left(h_0\frac{k}{\kappa^2}E\right)_{,x} + \frac{k}{h_0}\left(h_0\frac{l}{\kappa^2}E\right)_{,y} \quad (16)$$

$$\mathcal{F}_y = \frac{l}{h_0}\left(h_0\frac{k}{\kappa^2}E\right)_{,x} + \frac{l}{h_0}\left(h_0\frac{l}{\kappa^2}E\right)_{,y} \quad (17)$$

Here $\kappa^2 = |\vec{k}|^2$. These estimates can be useful for scaling the magnitude of the vorticity deposition as a function of energy density. In our numerical experiments, the mean field vorticity is directly available, but equations 15 and 16 can be used to think about some simple cases, and to check the numerics. Moreover, these estimates allow extension of the numerical model results to the cases of stronger wave forcing than is allowed by the numerical model.

In the case of a normally incident wave ($l = 0$) with an envelope ($\frac{\partial}{\partial y} \neq 0$) over longshore-independent terrain (see Figure 5), the vorticity source term is

$$(\nabla \times \overline{u})_{,t} = -\frac{k}{h_0}(\frac{h_0}{k}E)_{,xy}. \quad (18)$$

Aside from factors which arise from topographic variation, the right hand side is due to the y-variation of energy density divergence $E_{,x}$. Hence $\nabla \times \overline{u} \sim T\frac{E}{XY} \sim T\frac{c_{00}^2}{h_0}\frac{\overline{h'^2}}{XY}$. Here X and Y are length scales for change of E, and T is the total forcing time. The presence of the cross-derivative and the sign of the result must be diagnosed from the situation. Since we expect the amount of energy dissipation to be proportional in some way to the amplitude, the vorticity signal is as in Figure 5.

In the case of an obliquely incident wave ($l \neq 0$) with no envelope ($\frac{\partial}{\partial y} = 0$) over longshore-independent terrain, the vorticity source term is

$$(\nabla \times \overline{u})_{,t} = -\frac{l}{h_0}(\frac{h_0 k}{\kappa^2}E)_{,xx} \quad (19)$$

The primary signal is in the rate of change along the x-axis of $E_{,x}$, but the scaling now includes a geometric factor: $\nabla \times \overline{u} \sim T\frac{kl}{\kappa^2}\frac{E}{X^2} \sim T\frac{lk}{\kappa^2}\frac{c_{00}^2}{h_0}\frac{\overline{h'^2}}{X^2}$. This idealized situation is depicted in Figure 6.

We conclude this section by noting a relevant result that D.H. Peregrine has obtained. He used the circulation integral to give the total change in vorticity that a parcel of infinitesimal extent experiences upon passing through a bore [1]:

$$\delta(\nabla \times \vec{u}) = \left[\frac{2h_2}{gh_1(h_1+h_2)}\right]^{\frac{1}{2}}\frac{dE_D}{dy} \quad (20)$$

Here, E_D is the energy dissipation rate at the bore, h_2 and h_1 are fluid depths to the right and left of the bore, respectively. We take $h_2 > h_1$ and the parcel crossing from left to right. There is an additional change Δ in vorticity due to the stretching of the parcel as it crosses the bore. Δ is proprtional to $(\frac{h_2}{h_1} - 1)(\nabla \times \vec{u})$. Notice the dependence on the along-bore change in energy dissipation.

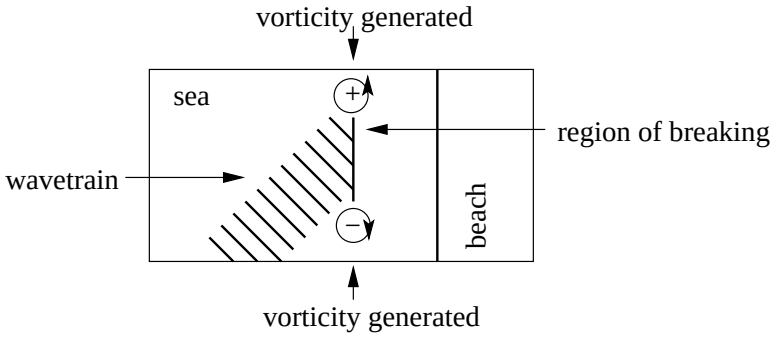

Figure 5: Enveloped incident waves. The component of the vorticity due to breaking which is associated with the envelope appears as the signed circles at the margins of the envelope.

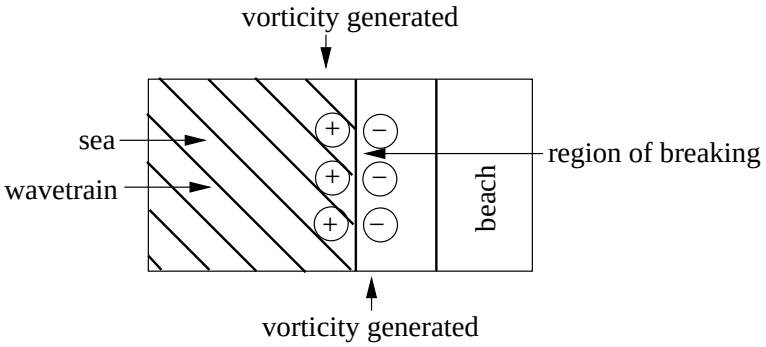

Figure 6: Unenveloped incident waves. The vorticity associated with the restriction of the breaking region to the region over the bar appears as the signed circles to the left and right of the bar.

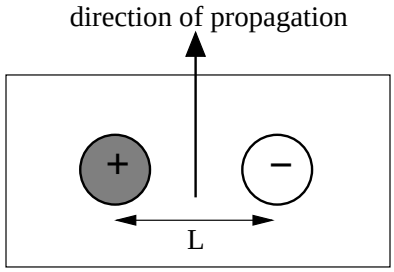

Figure 7: A vortex pair. Plan Form.

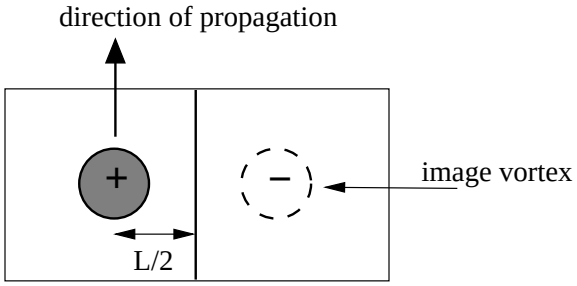

Figure 8: Vortex near a wall. Plan Form.

5 Vortex Dynamics

Consideration of the dynamics of a few typical vortical structures helps explain the motions associated with wave-induced mean-flow vorticity.

The motion of a vortex pair of opposite sign is perpendicular to the joining axis, see figure 7. The motion is in the direction indicated, with a velocity V which scales with S/L, where S is the vortex strength (i.e. circulation), and L is the separation. A typical timescale is $T \sim L/V = L^2/S$.

The motion of a single vortex adjacent to a wall is found from the method of images. It is just that of a vortex pair whose joining axis is perpendicular to the wall, and which has midpoint on the wall. (See Figure 8.)

The motion of a vortex on a slope is also found by a method of images: the vortex is completed to a vortex ring outside the domain. (Figure 9.) The vortex moves under the velocity field of this ring, perpendicular to the gradient of the slope. This result is not useful for a line vortex ring since such a ring moves with infinite velocity ([11]); instead, one should consider a distributed vortex patch. Stable vortex ring cross-sections are not known analytically, but one can estimate the speed of travel by cutting off the logarithmic divergence of the longshore velocity at the edge of the vortex core.

The distributions of vorticity in figure 5 of the previous section is such that the vortex pair should move up-slope over the bar, and towards the beach. However, the vortices should separate as they move up-slope, and come together as they move down-slope, in correspondence with the motion of figure 9.

The vorticity distribution in figure 6 is such that there is no apparent self-advection of vorticity, but a jet is driven between left and right vortex line. This situation would be

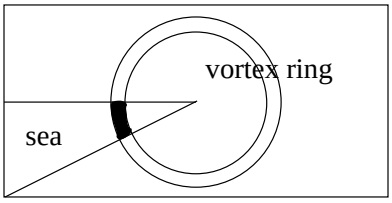

Figure 9: A vortex ring. The cross-section is the plane perpendicular to the axis of the beach. Motion of the vortex core is into or out of the page according to the sign of the vorticity.

unstable in the absence of mixing and bottom friction.

6 Numerical Results

We present two sets of results from the numerical experiments. The first is for the case of an obliquely incident wavetrain incident on a barred beach, and corresponds to the idealization of Figure 5. The second is the y-homogeneous case of Figure 6, again on a barred beach.

6.1 Numerical Model

The model is a shock-resolving finite-volume shallow-water solver built for this project. It uses a second-order time-stepping method, with the inter-cell fluxes computed by a Roe-approximate scheme. The topographic momentum source terms are handled with a splitting scheme. The CFL number is mantained at 0.95 throughout, with wavespeeds updated after each time-step. The waves are generated at the left side of the computational domain by an irrotational momentum forcing, derived from a potential. The forcing site introduces negligible vorticity into the simulations. The forcing generates a left- and a right-propagating wavetrain. The rightwards-moving wavetrain survives to break at the bar, but the other is removed by a damping layer at the left edge of the computational domain. The right side of the computational domain is a reflecting boundary condition. All runs were performed with shallow water ($< 0.1h_{max}$) near this right edge, so that waves of significant amplitude are removed by breaking at this location. The model is periodic in the longshore direction. The model has two major limitations. Only small-amplitude waves ($h'/h_0 \sim 0.01$) can be used, since waves of a larger order of magnitude shock fully after a single wavelength. This is in contrast with ocean waves, which experience no difficulty in propagating through deep water, only to break with $O(1)$ nonlinearity in the surf zone. Second, the requirement that the model resolve gravity waves led to small time-steps, so that integration of the vortex dynamics became computationally expensive. Pertinent information about the model runs is summarized in Table 1.

6.2 Enveloped oblique wavetrain

In this model run, a wavetrain is incident on the bar at an angle of 74 degrees from the normal. Figures 6.2 shows a contour plot of the free surface height. The PV field and the

Type	k	l	k_{abs}	Frequency	Envelope (half-width)	Amplitude
Enveloped	π	0.3π	1.044π	1.044π	6	0.01
Homogeneous	π	0.5276π	1.131π	1.131π	None	0.01

Table 1: Computations with and without envelope.

longshore current appear also in figure 6.2. Notice the appearance of the dipolar vorticity signal and its subsequent self-advection into the trough region. The longshore current is itself a consequence of another vortical dipole structure, though this is visible only in the tilting of the much stronger cross-shore-axis dipole. The average longshore velocity maximum clearly moves into the trough, though the average velocities are pathetic compared with local mean flow velocities (Figure 6.2). Much larger incident wave amplitudes would be needed to generate the longshore currents seen in the real surf zone, though whether the overall structure of the flow would be maintained in this case is unclear. In any case, this is the mechanism proposed for the presence of longshore currents in the trough. Ultimately the vortex pair curls up at heads which separate on the shore slope of the beach. They begin to feel the periodicity of the domain (Figure 6.2). At this point, the applicability of the model is ended and the run is termianated.

6.3 Homogeneous oblique wavetrain

This case has a homogeneous wave structure incident at 60 degrees from the normal. This case is intended as a check against the experimental work of Reiners and Battjes. [5]. The wavefield develops significant interaction with the mean flow after some initial development (Figure 13). Likewise, an intially extremely clean signal of PV its longshore jet are seen to become unstable in time. (Figure 14) The experimental work in [5] shows little evidence of this instability, but that work included bottom friction and momentum diffusion as an experimental matter of course, but such things as are not present in the numerics. The numerically produced longshore currents remain of lower amplitude (by a factor of six) than those of Reiners and Battjes, but half of this disagreement disappears when the numerical results are rescaled by $\sqrt{g}$ to include gravity in the shallow-water wave speed. If the jet had been stabilized by dissipation and forced at a higher wave amplitude, a result close to that of the experimental work might have been obtained. However, the forced-dissipative regime may be rather different from the numerical regime.

7 Conclusion

The main limitations of the numerical model are its inability to deal with large amplitude waves, and its failure to include dissiption and an eventual forced-dissipative equilibrium. The latter effect is easily incoporated into the model and should be included in any future work. The problem of amplitude is probably best approached by considering scaling arguments with respect to the wave amplitude h'. Questions of three-dimensional structure may be of interest, but lie beyond the scope of this study. The same is true of issues regarding the space- and time-distributions of incident waves. Such effects could be incorporated in

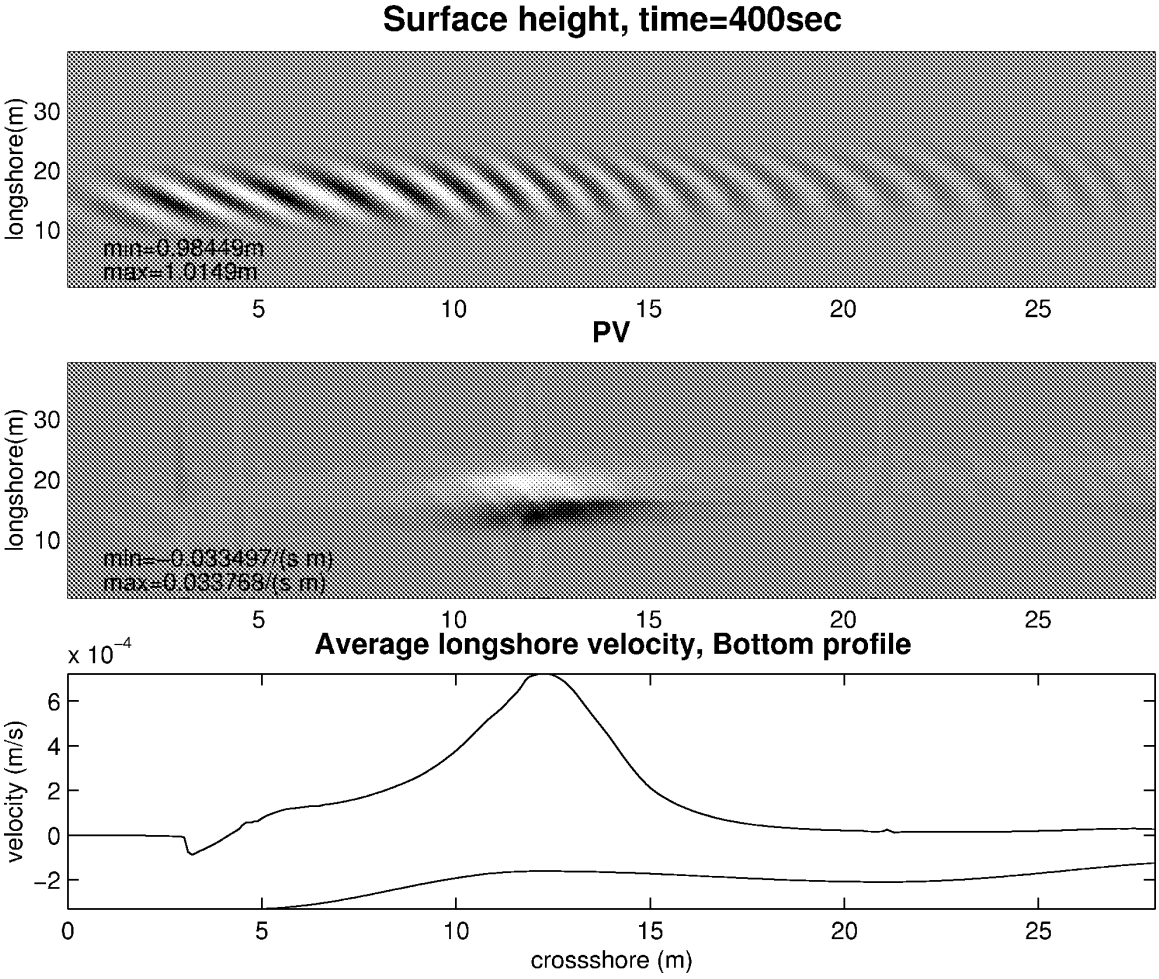

Figure 10: The enveloped oblique wavetrain. (See section 6.2.) A view of the height, PV, and average velocity in the early stage of development...

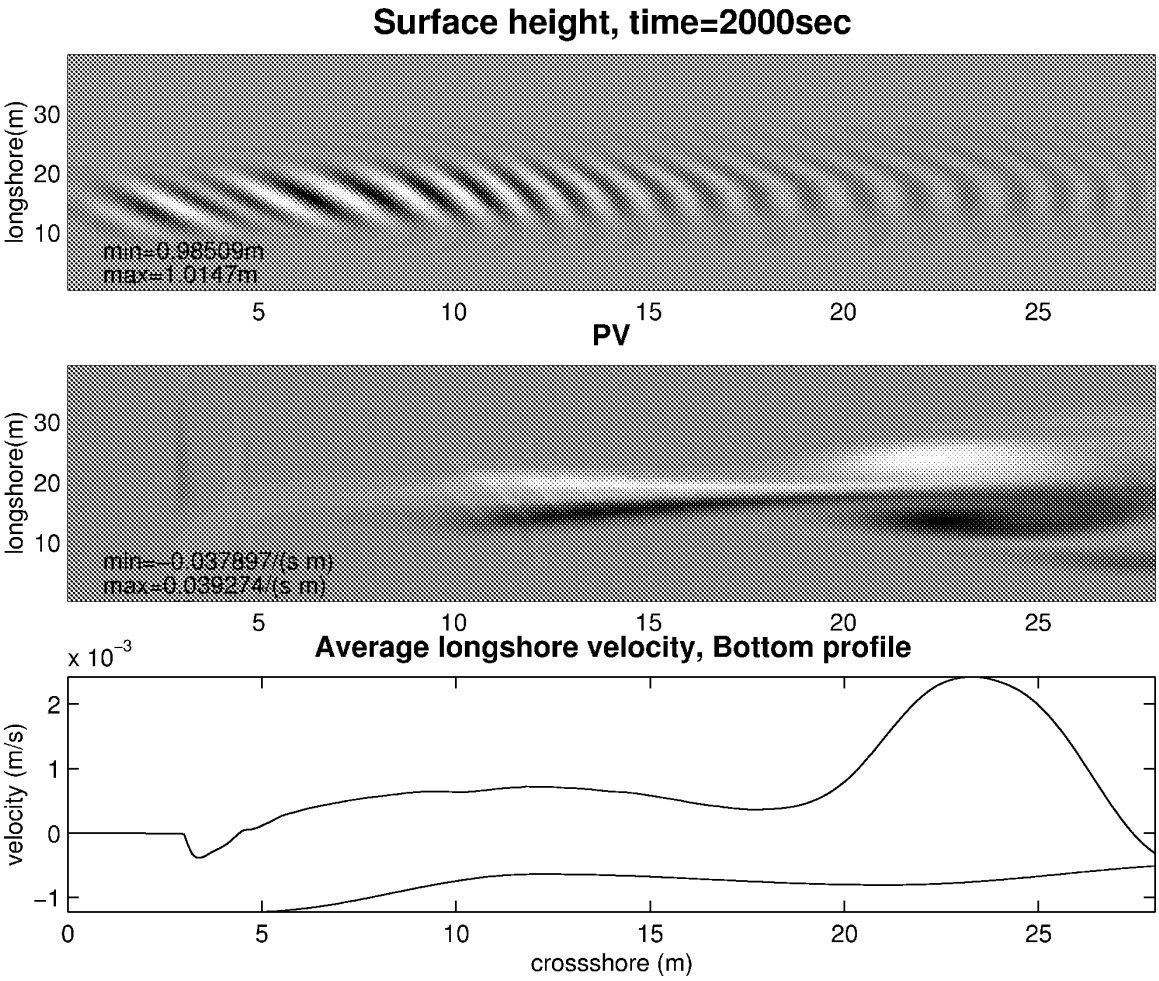

Figure 11: ...later...

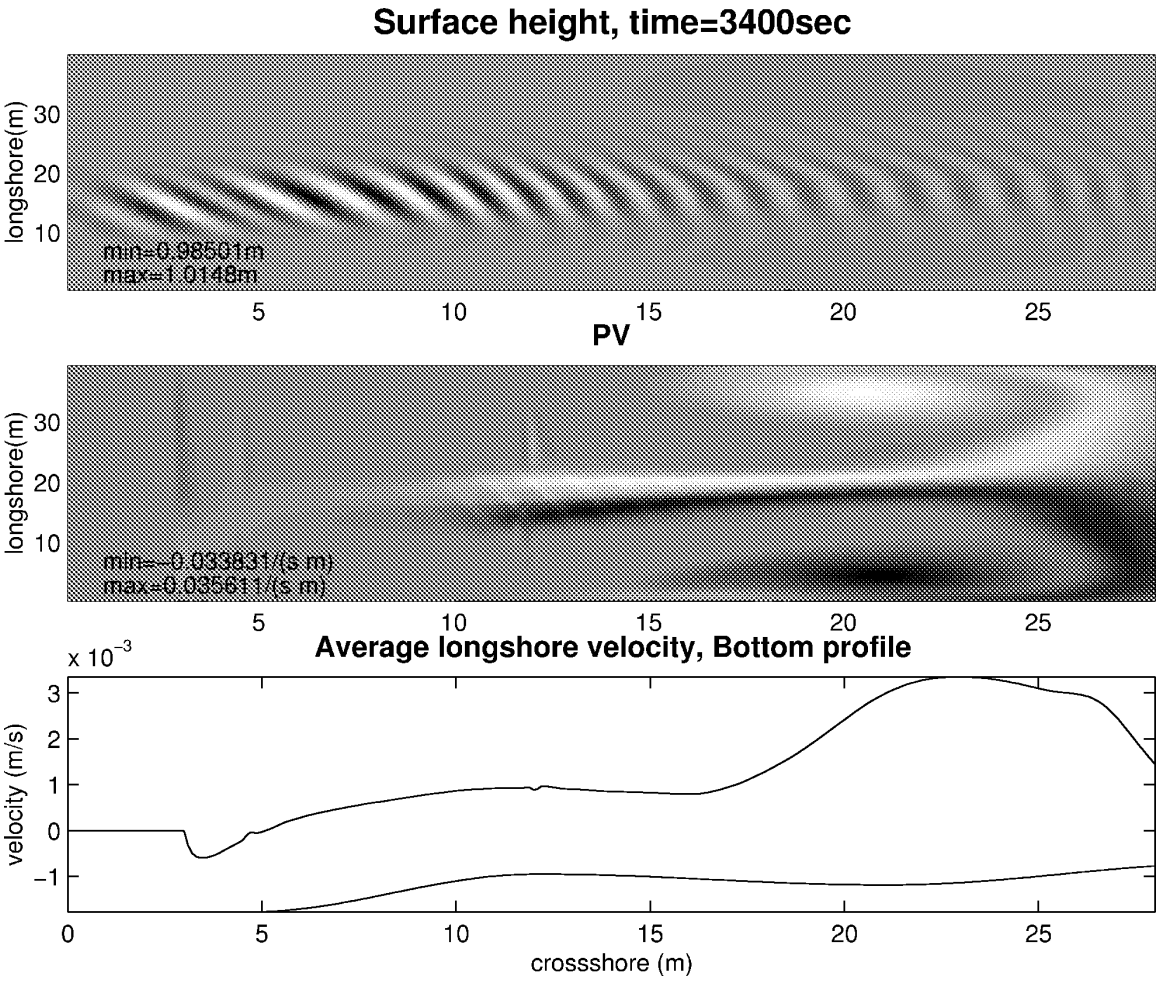

Figure 12: ...right before model termination.

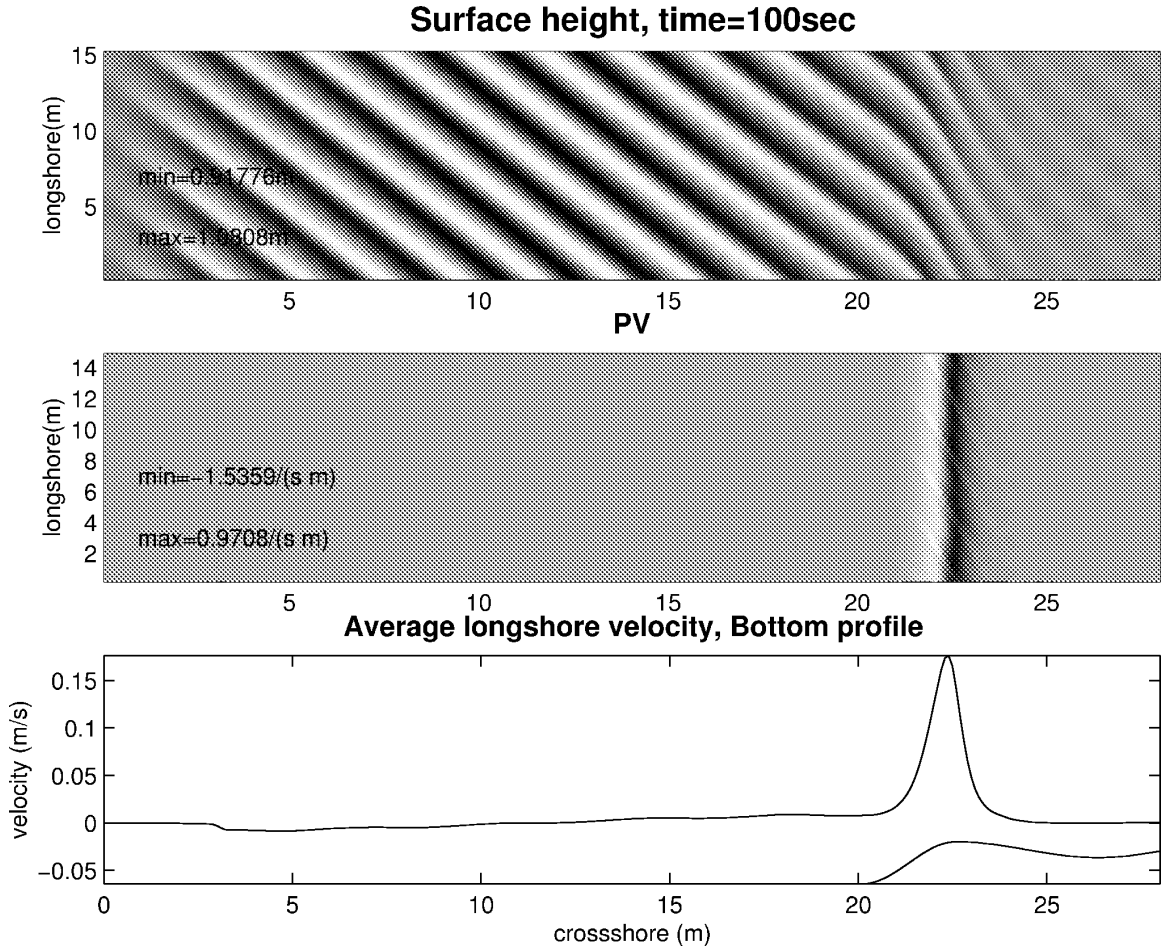

Figure 13: The homogeneous oblique wavetrain. (See section 6.3.) A view of the height, PV, and average velocity in the early stage of development...

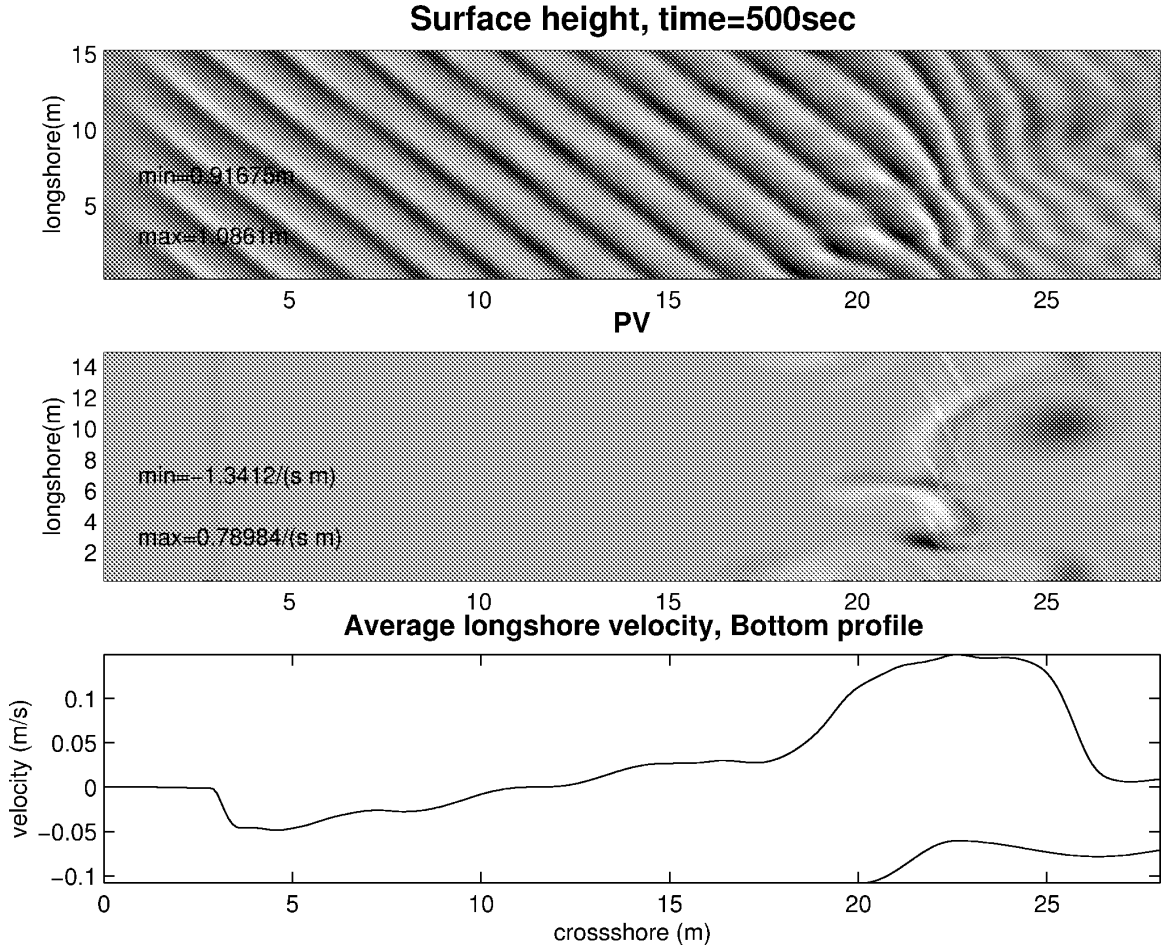

Figure 14: ...after the jet has grown unstable.

the numerical model, but are computationally much more demanding. Typical integration times for this model were already on the order of 10-20 hours.) An interesting topic for future research would be an attempt, probably based at first on a WKB approximation and a breaking parameterization, to identify interesting coupled wave-mean interactions. One could also consider the motion of the sand bars as a further mediation between wave and mean.

References

[1] D. H. Peregrine, "Surf zone currents," Theoretical and Computational Fluid Dynamics **10**, 295 (1998).

[2] D. H. Peregrine, "Large scale vorticity generation by breakers in shallow and deep water," Eur. J. Mech. B/Fluids **18**, 403 (1999).

[3] F. Feddersen (unpublished).

[4] J. C. Church and E. B. Thornton, "Effects of breaking wave induced turbulence within a longshore current model," Coastal Engineering **20**, 1 (1993).

[5] A. H. J. M. Reniers and J. A. Battjes, "A laboratory study of longshore currents over barred and non-barred beaches," Coastal Engineering **30**, 1 (1997).

[6] G. B. Whitham, *Linear and Nonlinear Waves* (John Wiley and Sons, New York, 1974).

[7] O. Bühler, "On the vorticity transport due to dissipating or breaking waves in shallow-water flow," J. Fluid Mech. **407**, 235 (2000).

[8] D. G. Andrews and M. E. McIntyre, "On wave-action and its relatives," J. Fluid Mech. **89**, 647 (1978).

[9] D. G. Andrews and M. E. McIntyre, "An exact theory of nonlinear waves on a lagrangian-mean flow," J. Fluid Mech. **89**, 609 (1978).

[10] O. Buhler and M. E. McIntyre, "On non-dissipative wave-mean interactions in the atmosphere or oceans," J. Fluid Mech. **354**, 301 (1998).

[11] G. K. Batchelor, *An Introduction to Fluid Dynamics* (Cambridge University Press, Cambridge, 1967).